Investigating neutral and stable atmospheric surface layers using computational fluid dynamics [†]

Fraser Gemmell [1,*]

[1]   Affiliation: Independent Researcher; fraser_gemmell@hotmail.com
*   Correspondence: fraser_gemmell@hotmail.com
[†]   Presented at ECAS, July 2021.

Abstract: Computational fluid dynamics (CFD) is an effective technique to investigate atmospheric processes at a local scale. For example, in near-source atmospheric dispersion applications, the effects of meteorology, air pollutant sources, and buildings can be included. A prerequisite is to establish horizontally homogeneous atmospheric conditions, prior to the inclusion of pollutant sources and buildings. This work investigates modelling of the atmospheric surface layer under neutral and stable boundary layer conditions, respectively. Steady-state numerical solutions of the Reynolds Averaged Navier-Stokes (RANS) equations were used, including the k-ε turbulence model. Atmospheric profiles derived from the Cooperative Atmosphere-Surface Exchange Study-99 (CASES-99) were used as reference data. The results indicate that the observed profiles of velocity and potential temperature can be adequately reproduced using CFD, while turbulent kinetic energy showed less agreement with the observations under the stable conditions. The results are discussed in relation to the boundary conditions and sources, and the observational data.

Keywords: CFD; Atmospheric Surface Layer; CASES-99; MOS

1. Introduction

Computational fluid dynamics (CFD) is an effective technique to investigate atmospheric processes at a local scale. For example, in near-source atmospheric dispersion applications, the effects of meteorology, air pollutant sources, and buildings can be included. In order to investigate local processes in CFD it is necessary to simulate an atmospheric surface layer. A prerequisite is to establish horizontally homogeneous atmospheric conditions, prior to the inclusion of pollutant sources and buildings.

Compared to neutral atmospheric conditions, a stable boundary layer (SBL) can suppress dispersion of emissions due to negative buoyancy effects, while an unstable boundary layer can enhance dispersion. This work investigates modelling of the atmospheric surface layer under neutral and SBL conditions, respectively.

It is a difficult process to model a realistic atmospheric boundary layer in CFD [1-3]. In addition, difficulties can arise due to unknown profiles of turbulence properties needed for modelling [4]. Under a SBL, shallow surface layers can occur, perhaps less than 10 m in depth, and it may be necessary to consider a much deeper layer. Several processes in the SBL can make this case much more difficult to investigate than neutral or unstable situations, including weak and intermittent turbulence, the production of elevated turbulence, and other phenomena [5-7].

The objective here was to attempt to establish a horizontally homogeneous atmospheric surface layer with the numerical model; whereby the inlet velocity and turbulence profiles, the ground shear-stress and turbulence model are in equilibrium. An approach for this under a neutral atmosphere is well established [4] and is adopted here. An attempt is also made here to apply a similar approach to a SBL. For both neutral and

stable atmospheres, the assumption was made that pressure was constant in the domain, and flow was driven by a shear stress at the top of the surface layer.

This paper is structured as follows. First, the CFD equations describing the situation are described. The numerical methods and the boundary conditions are then summarized. The CASES-99 data are described, as is the Monin-Obukhov similarity (MOS) theory which is used to provide profiles of velocity and temperature as upwind boundary conditions for CFD. Details of the approaches used to simulate both the neutral and the stable surface layers are given, followed by the results and discussion.

2. Materials and Methods

2.1 CFD equations and numerical methods

A steady-state numerical solution has been used in CFD modelling of the surface layer [1-4]. For this work, the OpenFOAM steady-state solver for turbulent compressible flows was adapted, which includes solution of the conservation, momentum, turbulence, and enthalpy equations respectively [8]. Temperature is calculated from enthalpy using a numerical scheme [9]. The momentum and turbulence equations are given below, in order to show the specific terms used here.

The momentum conservation equation is given by [9]:

$$\frac{\partial(\rho\boldsymbol{u})}{\partial t} + \nabla \cdot (\rho\boldsymbol{u}\boldsymbol{u}) = -\nabla p + \boldsymbol{g}(\rho - \rho_0) + \nabla \cdot (2\mu_{eff}D(\boldsymbol{u})) - \nabla\left(\frac{2}{3}\mu_{eff}(\nabla \cdot \boldsymbol{u})\right) \tag{1}$$

where **u** is the velocity vector; ρ is the density; p is the pressure; and μ_{eff} is the sum of the molecular (μ_l) and turbulent viscosities (μ_t), respectively. The second term on the right-hand-side of Eq. (1) is the buoyancy source term applied here, in which **g**=[0, 0, -9.8 m s^{-2}]; ρ_0 is the reference density at $\Theta_0(z)$, given by the lapse-rate of potential temperature. For neutral conditions, Θ_0 is constant. The rate of strain tensor D(**u**) is defined as:

$$D(\boldsymbol{u}) = \frac{1}{2}((\nabla \boldsymbol{u}) + (\nabla \boldsymbol{u})^T)$$

The standard k-ε model was used to model turbulence [10]. k is the turbulent kinetic energy and ε is the turbulent dissipation rate:

$$\frac{\partial(\rho k)}{\partial t} + \nabla \cdot (\rho\boldsymbol{u}k) = \nabla \cdot \left(\frac{\mu_{eff}}{\sigma_k}\nabla k\right) + P_k + G_b - \rho\varepsilon \tag{2}$$

$$\frac{\partial(\rho\varepsilon)}{\partial t} + \nabla \cdot (\rho\boldsymbol{u}\varepsilon) = \nabla \cdot \left(\frac{\mu_{eff}}{\sigma_\varepsilon}\nabla \varepsilon\right) + \frac{\varepsilon}{k}(C_1 P_k + C_3 G_b - \rho C_2 \varepsilon) \tag{3}$$

$$\mu_t = \frac{\rho C_\mu k^2}{\varepsilon} \tag{4}$$

$$P_k = \mu_t \left(\frac{\partial u_i}{\partial x_j} + \frac{\partial u_j}{\partial x_i}\right)\frac{\partial u_i}{\partial x_j} \tag{5}$$

$$G_b = -\mu_t \frac{\boldsymbol{g} \cdot \nabla \rho}{\rho\sigma_{t,h}} \tag{6}$$

where, P_k is the volumetric production rate of k by shear forces; G_b is the volumetric production rate of k by buoyancy forces; $\sigma_{t,h}$ is the turbulent Prandtl number ($\sigma_{t,h}$=1.0, [11]); σ_k is the turbulent Prandtl number for k (σ_k=1.0); σ_ε is the turbulent Prandtl number for ε (σ_ε=1.31). The constants are: C_μ=0.09, C_1=1.44, C_2=1.92. G_b is negative for stably stratified flows, so that k is reduced and turbulence damped. For unstably stratified flows, G_b is positive and k increases [12]. The coefficient C_3 depends on the flow situation. In this work, a value of C_3=-0.8 was used [4].

OpenFoam uses the finite-volume method, whereby the terms in the conservation equations are discretized by integrating over the cell volume. The upwind-differencing scheme was used for the convective terms [13]. The discretized equations were solved using standard linear solver methods in OpenFoam. Pressure and velocities were coupled in the solution process using the SIMPLE algorithm [13]. The imbalances in the fi-

nite volume equation (the residuals) were used as a measure of the quality of the solution at each step in the iterative process. Iterations stop when the residual errors sum to less than user-set tolerances.

The key boundary conditions included: (i) upwind boundary: the appropriate vertical profiles of the relevant variables were set here, including velocity, potential temperature, k, and ϵ. (ii) downwind boundary: a fixed-pressure condition was applied, with an inlet-outlet condition for velocity. The inlet-outlet condition provides a zero-gradient condition for velocities, if outflow occurs, and fixed-value conditions on inflow. A fixed-pressure condition was applicable, since the variation of pressure due to hydrostatic effects was not included. (iii) ground surface: an atmospheric rough-wall function was applied. (iv) upper boundary: a fixed-pressure condition with an inlet-outlet condition for velocities was applied.

Simulations based on the finite volume method with flux defined boundary conditions (Neumann type) usually encounter numerical problems due to the backwards propagation of physical characteristics during the simulation procedure [4]. Fixed-temperature values (Dirichlet type) on both boundaries have been suggested as a compromise solution [4]. Fixed-temperature boundaries were used here at ground surface and at the upper-boundary, respectively. In a stably stratified condition, the heat flux is oriented downwards from upper to lower boundary and the value of the heat flux at the ground surface is negative.

2.2 CASES-99 data

Near-surface profile data from CASES-99 [14] were used in this work. Data were obtained in netCDF format from EOS/NCAR [15]. The data were from the main CASES-99 60 m flux tower, and comprised 5-min averages of means, variances and covariances of the ISFF variables. Wind and temperature measurements on the 60 m tower were conducted by sonic anemometers at heights of 1.5, 5, 10, 20, 30, 40, 50, and 55 m [6]. This provided 3-component wind and temperature data at a sampling rate of 20 Hz. A number of low surface wind-speed situations were examined, and the profile data selected for the present work were from 18/10/1999 0900-0930 UTC, using a 30 min average. Wind-speed at a height of 1.5 m was 1.3 m/s, and a distinct temperature inversion existed. Wind and temperature profiles were found to be relatively steady over the course of the selected period. The virtual temperature profile data were adjusted by the dry adiabatic lapse-rate, to obtain potential temperature (Θ) values. Dry air was assumed in the modelling. The roughness length used for the tower site was z_0=0.03 m [16]. Wind vectors from the sonic anemometers were provided as rotated from instrument coordinates to normal meteorological coordinates. These data were converted to give the mean wind speed. Friction velocity (u_*=0.12) and temperature scale (Θ_*=0.07) were also needed for this work, and were obtained using the respective covariance values measured at the surface as follows [7]:

$$u_{star} = \left[\left(- \overline{u'w'} \right)^2 + \left(- \overline{v'w'} \right)^2 \right]^{(1/4)} \tag{7}$$

$$\theta_{star} = \frac{\overline{w'\theta'}}{- u_{star}} \tag{8}$$

Turbulent kinetic energy (k) was obtained as:

$$k = \frac{1}{2} \left(\overline{u'^2} + \overline{v'^2} + \overline{v'^2} \right) \tag{9}$$

2.3 MOS

It was attempted to reproduce the measured profiles of wind speed and Θ using MOS flux-profile relationships [5]. The aim was to apply the MOS derived profiles as upwind boundary conditions. Flux-profile relationships relate the surface turbulent flux of momentum and heat to their respective profiles of mean wind speed and temperature [6]. When the turbulence covariances are not available, then turbulent fluxes of momen-

tum and heat can be estimated from vertical profiles of mean values of wind speed and Θ
using MOS [2, 17]. The MOS profiles of wind speed and Θ are, respectively [5]:

$$u(z) = \frac{u_{star}}{\kappa}\left[\ln\left(\frac{z}{z_0}\right) + \Psi_M\left(\frac{z}{L}\right)\right]$$

(10)

$$\theta(z) = \frac{\theta_{star}}{\kappa}\left[\ln\left(\frac{z}{z_0}\right) + \Psi_T\left(\frac{z}{L}\right)\right]$$

(11)

$$L = \frac{u_{star}^2 \theta_s}{\kappa g \theta_{star}}$$

(12)

where, $\Psi_M = \Psi_T = 4.7\ z/L$; L is the Monin-Obukhov length; $\kappa = 0.41$ is the von Karman constant; $u(z)$ is wind speed; $\Theta(z)$ is the potential temperature; and Θ_s is the surface temperature. For the case of neutral stability, only Eq. (10) is relevant with $\Psi_M = 0$.

L is a measure of the height of the dynamical influence layer where surface properties are transmitted [7]. The surface layer height of a stable stratification is the same order as L [18]. For $z > L$, thermal influences are the dominant factor. In the present case, the value of L obtained was 14 m. Thus, the CASES-99 measurements taken at 20 m and above were not in the immediate surface layer, so may have been decoupled from surface influences to some extent. MOS assumes that the shear stress and heat flux are constant in the surface layer [2].

The MOS estimated profiles of horizontal velocity and Θ for the SBL are shown below in Figure 2 (a) and (b), respectively. A reasonable agreement between MOS and the measurements was obtained. It can be seen that the vertical structure of Θ was more complex than the MOS profile. The numerical simulations described next, are an attempt to replicate the MOS profiles.

2.4 Experimental procedure

The simulations were carried out in 2-D since the flow properties were invariant in the y-direction, but results were also confirmed in 3-D for selected cases. The test domain size was based on a scale suitable for near-surface dispersion modelling being 3000 m in length and 100 m in height. For the 3-D cases, a 40 m wide domain was used. The number of grid cells was: x (200), y (10), z (50), with gradation in the z-direction used to give greater resolution near the ground surface. The first cell centre was located at a height of 0.15 m.

For the neutral case, the whole 100 m depth of the domain was contained in the surface layer, and the shear stress was assumed constant through the layer, equalling the shear stress at the surface. The approach taken for the neutral atmosphere applies analytic solutions to the momentum and turbulence equations as the upwind boundary conditions; and maintains a horizontally homogeneous atmosphere through the use of sources of momentum and ε, applied at the upper boundary, and a rough wall function applied at the ground surface [1]. In order to satisfy the analytic solution, a different value of $\sigma_\varepsilon = 1.11$ is used [1]. This approach ideally results in a logarithmic wind profile, a zero-vertical velocity, and constant values of k, Θ, and pressure, respectively, everywhere in the domain. For the neutral case, the value of $u_* = 0.12$ obtained above for the SBL, was used to provide the required value of u_*, which determines the upwind profiles of wind speed, k, and epsilon [1]. This allowed both neutral and stable cases to be put on a common reference scale. However, u_* reflects different relative magnitudes of mechanically- and buoyancy-driven turbulence in each atmosphere.

For the SBL case, the approach taken was similar, with the upwind boundary conditions given by MOS, and a rough wall function applied at the ground surface. However, two difficulties existed compared to the neutral case. First, with the surface layer depth of only 14 m, the way to model the situation was less clear. One possibility was to attempt to model only the lower 14 m or so in the SBL case; however, this would not be of much practical use in applications, where buildings are often higher than this for ex-

ample. The turbulent shear stress at the top of domain was not known, but the CAS-ES-99 observation data indicated it may have been zero. Figure 2 (e) shows that the observed shear stress fell from its surface value to zero at about 40 m. Thus, for the SBL, no source of momentum was applied at the upper boundary.

Second, known profiles for k and ε were not available for the SBL. If the measured profile of k was used, it was not sustained by the current model configuration which included the k-ε model, the boundary conditions, and numerical methods used. Thus, a different approach was taken in order to estimate the upwind boundary conditions for k and ε. The most consistent boundary conditions with respect to the applied equation system are the numerical results [4]. For a fixed bulk velocity, the turbulence characteristics can be obtained from the equilibrium state, as it results from the interaction of turbulent shear and inertial force [4]. Equilibrium profiles for k and ε were obtained here by running simulations on a domain 10 km in length, that is, beyond the distance where profiles were changing downwind. The resulting profile of k is shown in Figure 2 (c).
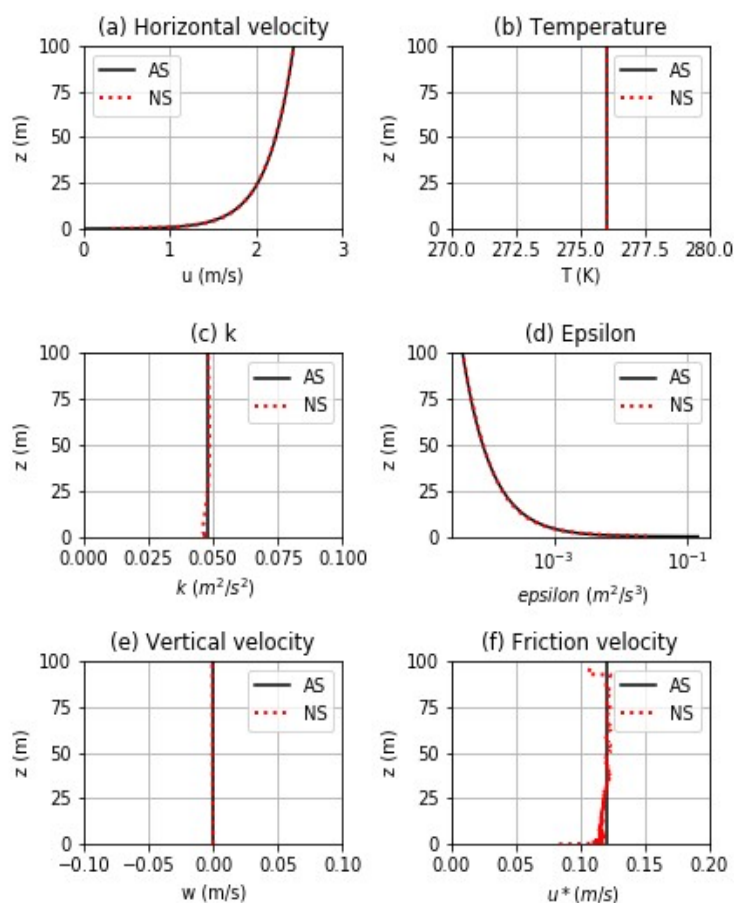

Figure 1. Comparison of the numerical solution (NS) with the analytic solution (AS) for the neutral atmosphere. (a) horizontal velocity; (b) potential temperature; (c) turbulent kinetic energy; (d) turbulence dissipation rate; (e) vertical velocity; (f) friction velocity. The numerical results are shown for a position 2000 m from the upwind boundary of the domain.

3. Results

Figure 1 shows the results for the neutral atmosphere. It can be seen that the numerical results compare well with the analytic solutions for all variables. The velocity and Θ profiles were maintained along the whole 3 km domain length. Although the analytic k profile was used as the upwind boundary condition, the k profile took some distance to stabilise to its equilibrium form, but was sustained thereafter along the remaining length

of the domain. Work is being aimed at better understanding this situation, including the initial values used and other numerical factors. The results indicated that the velocity and Θ profiles were relatively insensitive to the specific form of the k profile. This may be because turbulence is a second order effect.

Figure 2 shows the results for the SBL. The numerical results compare well with the MOS profiles for horizontal velocity and Θ in Figures 2 (a) and 2 (b), respectively. In addition, k matches its reference profile reasonably well in Figure 2 (c). At equilibrium, turbulence production and destruction should be in balance, that is $\varepsilon = P_k + G_b$, and it can be seen in Figure 2 (f) that the vertical profile of ε follows closely the production/destruction rates of k, indicating that equilibrium was attained. In summary, the numerical results generally were able to replicate the profiles derived from MOS based on the surface flux data.
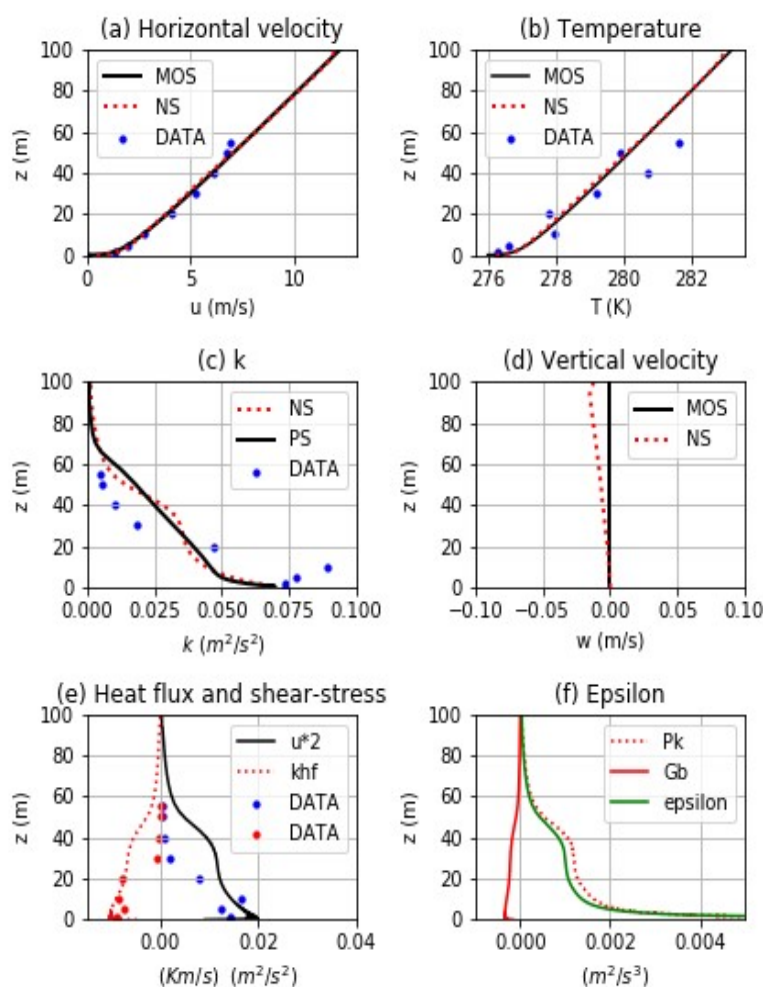

Figure 2. Comparison of the numerical solution (NS) with the reference profiles for the stable atmosphere. (a) horizontal velocity; (b) potential temperature; (c) turbulent kinetic energy. PS refers to the precursor simulation result; (d) vertical velocity; (e) kinematic heat flux and shear-stress; (f) numerical production and dissipation of k. The numerical results are shown for a position 2000 m from the upwind boundary of the domain. Also shown are the CASES-99 data, where applicable.

4. Discussion

In contrast to the neutral case, it was found that the SBL profiles of horizontal velocity and k could be maintained without a shear stress applied to drive the flow. The reason for this is not fully understood at this point, however a small negative vertical velocity was found in the solution in the top of the domain (Figure 2 (d)) – so air at the

top velocity was being drawn into domain through the upper boundary. This advection appears to be balancing the shear stress convergence in the lower part of the domain.

The numerical k profile is quite different compared to the CASES-99 measurements, being under-predicted below 20 m and over-predicted above this height (Figure 2 (c)). It is not surprising that k does not capture the finer structure of the observations. No attempt was made to capture the specific detail of the observation at this stage; indeed such an attempt may be too ambitious, using the current approach.

Figure 2 (e) shows the modelled profiles of heat flux and shear stress, respectively. The CASES-99 observations of heat flux and shear stress are also shown. To some extent, a constant flux layer may be seen in the numerical results though it is deeper than the 14 m predicted by MOS, being around 40 m depth. This difference appears to be due mainly to the over-prediction of k centred at a height of around 40 m. Nevertheless, the result seems encouraging and suggests that with further refinements to the current approach, it may be possible to model the depth and nature of the surface layer more accurately.

A number of factors are being considered that might lead to a better prediction of k. The observations indicate that Θ increases with height at a greater rate than that predicted by the MOS-derived profile, as shown in Figure 2 (b). The magnitude of G_b may thus have been under-estimated, which could have led to greater modelled levels of k higher up in the domain, than were measured. This is one aspect that will be tested in further work. Another factor being considered is the value used for C3, which affects the impact of the destruction rate in the k-ε model. Significant existing work has gone into optimising the value of C3 [2]. Initial experiments in which different values of C3 were used has not yet shown any notable improvements in results for k.

Conflicts of Interest: The author declares no conflict of interest.

References

1. Richards, P. J. and Norris, S. E. Appropriate boundary conditions for computational wind engineering models revisited. *J. Wind. Eng. Ind. Aerodyn.* **2011**, *99*, 257-266.
2. Alinot, C. and Masson, C. k-epsilon model for the atmospheric boundary layer under various thermal stratifications. *J. Sol. Energy Eng.* **2005**, *127*, 438-443.
3. Yang, Y., Gu, G., Chen, S., Jin, X. New inflow boundary conditions for modelling the neutral equilibrium atmospheric boundary layer in computational wind engineering. *J. Wind. Eng. Ind. Aerodyn.* **2009**, *97*, 88-95.
4. Chang, C.-Y.; Schmidt, J.; Dorenkamper, M.; Stoevesandt, B. A consistent steady state simulation method for stratified atmospheric boundary layer flows. *J. Wind. Eng. Ind. Aerodyn.* **2018**, *172*, 55-67.
5. Stull, R. *An Introduction to Boundary Layer Meteorology*. Springer, New York, USA, 2009.
6. Cheng, Y.; Oarlange, M. B.; Brutsaert, W. Pathology of Monin-Obukhov similarity in the stable boundary layer. *J. Geophys. Res.* **2005**, *110*, 1-10.
7. Yague, C.; Viana, S.; Maqueda, G.; Redondo, J. M. Influence of stability on the flux-profile relationships for wind speed, φ_m, and temperature, φ_h, for the stable atmospheric boundary layer. *Nonlin. Processes Geophys.* **2006**, *13*, 185-203.
8. OpenFOAM. Available online: https://www.openfoam.com/ (accessed on 7 June 2021).
9. Nozaki, F. Available online: http://caefn.com/openfoam/solvers-buoyantpimplefoam/ (accessed on 7 June 2021).
10. Launder, B. E. and Spalding, D. B. The numerical computation of turbulent flows. *Comput. Method. Appl. M.* **1974**, *3(2)*, 269-289.
11. Li, D. Turbulent Prandtl number in the atmospheric boundary layer – where are we now? *Atmos. Res.* **2019**, 216, 86-105.
12. CHAM. Available online: http://www.cham.co.uk/phoenics/d_polis/d_enc/turmod/enc_t341.htm/ (accessed on 7 June 2021).
13. Versteeg, H.; Malalasekera, W. *An Introduction to Computational Fluid Dynamics: The Finite Volume Method*. Pearson Education Limited: Essex, England, 2007.
14. Poulos, G. S.; Blumen, W; Fritts, D. C.; et. al. CASES-99: A Comprehensive Investigation of the Stable Nocturnal Boundary Layer. *Bull. Amer. Meteor. Soc.* **2002**, *83*, 555-581.

15. 5 Minute Statistics of ISFF data during CASES-99 Version 1.0. 2016, UCAR/NCAR - Earth Observing Laboratory. Available online: https://www.eol.ucar.edu/field_projects/cases-99/ (accessed on 7 June 2021).

16. Vickers, D.; Mahrt, L. The Cospectral Gap and Turbulent Flux Calculations. *J. Atmos. Ocean Technol.* **2003**, *20*, 660-672.

17. Taylor, P.; Laroche, D.; Wang, Z-Q.; McLaren, R. Obukhov Length Computation using simple measurements from weather stations and AXYS Wind Sentinel Buoys. WWOSC, Montreal, Canada, 2014.

18. Emeis, S.; *Wind Energy Meteorology: Atmospheric Physics for Wind Power Generation*. Springer Science & Business Media, New York, USA, 2018.